# Scholarly Research Exchange

*Research Article*

# Structural and Optical Characterisation of an Erbium/Ytterbium Doped Hybrid Material Developed via a Nonhydrolytic Sol-Gel Route

**M. Oubaha,[1] R. Copperwhite,[1] C. McDonagh,[1] P. Etienne,[2] and B. D. MacCraith[1]**

[1] *Optical Sensors Laboratory, National Centre for Sensor Research, School of Physical Sciences, Dublin City University, Dublin 9, Ireland*

[2] *Groupe d'Etude des Semiconducteurs, Université de Montpellier 2, UMR-CNRS 5650, Place Eugéne Bataillon, 34090 Montpellier, France*

Correspondence should be addressed to M. Oubaha, mohamed.oubaha@dcu.ie

This paper proposes the development and structural characterisation of an $Er^{3+}/Yb^{3+}$ doped hybrid organic-inorganic material synthesised by a nonhydrolytic sol-gel process. By using a pumping laser diode at 980 nm, a typical $Er^{3+}$ luminescence has been recorded in the near infrared region (1.53–1.55 $\mu$m). However, the detected fluorescence was particularly weak compared to that generally observed in pure mineral materials, suggesting the occurrence of strong quenching due to multiphonon relaxation processes. To understand this behaviour, structural characterisation of both of the matrix and the local environment of $Er^{3+}$ ions were conducted employing infrared spectroscopy, nuclear magnetic resonance, electron paramagnetic resonance, and neutron scattering. These studies showed that the major phenomenon competing with the $Er^{3+}$ fluorescence is intimately associated to the strong vibrational modes of the organic species that involve multiphonon relaxation processes, resulting in energy dissipation within the host matrix.

## 1. Introduction

Since the early 1990s hybrid organic-inorganic has been very popular for the development of novel materials with tuneable properties and morphologies.

In particular, Ormosils (organically modified silicon) $(R'xSi(OR)4-x)$ synthesised by the sol-gel process [1] have been widely studied for the preparation of hybrid organic-inorganic materials for different applications such as separation [2, 3], sensing [4, 5], surface protection [6, 7], and optics [8–12].

In the optics field, an exciting challenge was the development of integrated optical devices that allow the integration of several functions on one chip, which has become possible for example by combining a photolitographic process with photocurable hybrid sol-gel materials [12, 13].

However, to our knowledge, the fabrication of active integrated optical circuits employing photocurable hybrid sol-gel materials has not been reported previously, despite their great potential to enable the use of large bandwidth lasers. One of the major challenges in the development of $Er^{3+}$ doped hybrid materials for optical amplification around 1550 nm is the avoidance of OH groups in the material. Unfortunately, these groups are inherent to the hydrolytic sol-gel process and are well known to compete with the $Er^{3+}$ luminescence by nonradiative decay processes [14, 15].

In this paper, we report the development of a novel OH-free $Er^{3+}/Yb^{3+}$ codoped photocurable material employing a nonhydrolytic sol-gel route. The spectroscopic behaviour of the active dopants is correlated to the structure of the host matrix by means of near infrared spectroscopy (NIR), nuclear magnetic resonance (NMR), electron paramagnetic resonance (EPR), and neutron scattering.

## 2. Experimental

*2.1. Material.* In order to avoid any relaxation due to the OH groups, inherent to the hydrolytic sol-gel route, the goal of the material synthesis consists of obtaining an OH-free condensed organo-silane. To achieve this, the sol-gel synthesis was conducted via a nonhydrolytic sol-gel process, as sketched in Figure 1.
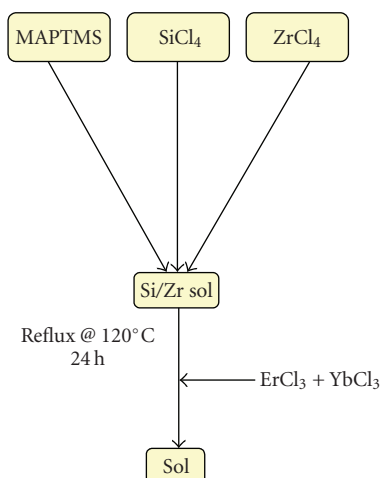
FIGURE 1: Nonhydrolytic sol-gel synthesis of a photocurable organosilane material.

Compared to the hydrolytic routes, which can be processed at ambient temperature, nonhydrolytic processes typically require higher temperature and a catalyst to allow the condensation reaction between precursors of different reactivity. Generally, to condense an alkoxysilane with a chlorosilane, a Lewis acid catalyst, such as zirconium tetrachloride ($ZrCl_4$) is employed [16].

The sol preparation consisted of mixing a photocurable organically modified silicate, 3-trimethoxypropyltrimethoxysilane (MAPTMS, Assay ~99%) together with silicon tetrachloride ($SiCl_4$, Assay ~99.99%) in the presence of zirconium tetrachloride ($ZrCl_4$, Assay ~99.99%). The mixture was refluxed at 120°C for 24 hours before addition of the doping elements $ErCl_3$ and $YbCl_3$. The obtained sol was then filtered, through a 0.2 micrometer membrane, to remove any contaminating particle. NIR and neutron scattering spectra were recorded on bulk samples of 2 to 5 millimetre thicknesses. For EPR, the solid gels were crushed and the resulting powders sealed under vacuum into glass tubes.

*2.2. Experimental Techniques.* The evolution of the siloxane hybrid network has been followed by $^{29}$Si-NMR spectroscopy, employing a 400 MHZ Bruker spectrometer. The various oxo bridges formed through either self-condensation or cocondensation reactions between the MAPTMS and the $SiCl_4$ are easily identified during the synthesis. Spectra were recorded at room temperature from liquid solution. Measurements showed that a 4-second recycle delay time with an 8 $\mu$s pulse duration, was sufficient for quantitative measurements. The chemical shifts were referenced with respect to Tetramethylsilane, used as an external reference. The Free Induction Decay processing used a 10 Hz line broadening. Each recorded spectrum is an average of all previously obtained spectra during the instrument acquisition time. 128 scans were accumulated for each spectrum.

NIR is commonly used to identify the absorption of the harmonics and combinations bands of the fundamental

vibrations as well as the absorption of rare earth ions [17]. In the present case, this technique was employed to identify the optimum excitation wavelength of $Er^{3+}$ and quantify the effect of the $Yb^{3+}$ codoping effect. NIR spectra were performed using a NIR spectrometer. This optical spectrum analyser included an infrared source, a second-order blocking filter, and a scanning monochromator with both Ge (600–1900 nm) and PbSe (1500 and 3000 nm) detectors. The resolution can be selected between 0.25 and 20 nm. The scanning monochromator used a continuously rotating diffraction grating driven by an electronically controlled DC motor.

EPR spectroscopy characterises the environment of the paramagnetic species (in this case $Er^{3+}$). In this work, this technique was used to investigate the homogeneity of the sample as function of $Er^{3+}$ concentration. EPR spectra were recorded at room temperature employing an ER200D (X band) spectrometer operating at 9 GHz.

Compared to light scattering, which yields information on particles of >100 nm, neutrons scattering allows structural characterisation on a smaller scale, typically from 10 to 500 Å. Neutrons scattering experiments were performed on the small angle neutron scattering spectrometer at the Orphée 14 MW Reactor at the French Atomic Energy (CEA Saclay, France), using a neutron wavelength of 50 Å.

Fluorescence emission measurements were performed at room temperature by optically pumping the samples with a Ti: sapphire laser tuned at 980 nm. The light emitted at 90° from the monolith was analysed spectrally with a Jobin-Yvon U1000 double-monochromator fitted with a grating of 600 grooves/mm. The fluorescence was detected by a North-Coast liquid-nitrogen-cooled germanium detector. The spectral resolution ranged from 1 to 2 nm. The pump signal was mechanically chopped at 80 Hz and the signal from the Ge-detector was preamplified and passed to a lock-in amplifier.

## 3. Results and Discussion

*3.1. $^{29}$Si-NMR.* The $^{29}$Si-NMR spectra of the pure MAPTMS and $SiCl_4$ alkoxides (not shown here) exhibit a single peak at $-42.8$ and $-19.2$ ppm, respectively. This is an indication of the high purity of the employed precursors and absence of any hydrolysed species.

Figure 2 shows the $^{29}$Si-NMR spectra after 1 hour and 24 hours of reaction. After 1 hour of reaction, in addition to the precursors peaks, two resonances located at $-36.5$ and $-27$ ppm are observed, with a respective contribution of 27.0 and 30.3% of the total silicon nuclei, as summarised in Table 1. After 24 hours of reaction, all peaks observed after 1 hour of reaction disappear with the appearance of 3 new peaks, located at $-49.1$, $-58$, and $-59$ ppm, and a large band between $-65$ and $-69$ ppm. This band is in fact composed of two main peaks centred at $-66$ and $-67.8$ ppm.

The noncondensed silicon nuclei ($T_0$ groups) are generally observed at chemical shifts lower than $-45$ ppm [18]. In a similar structure, the progressive condensation provoked an increase of 10 ppm [19, 20]. Based on the literature, it is possible to confirm that the peaks observed in the sample
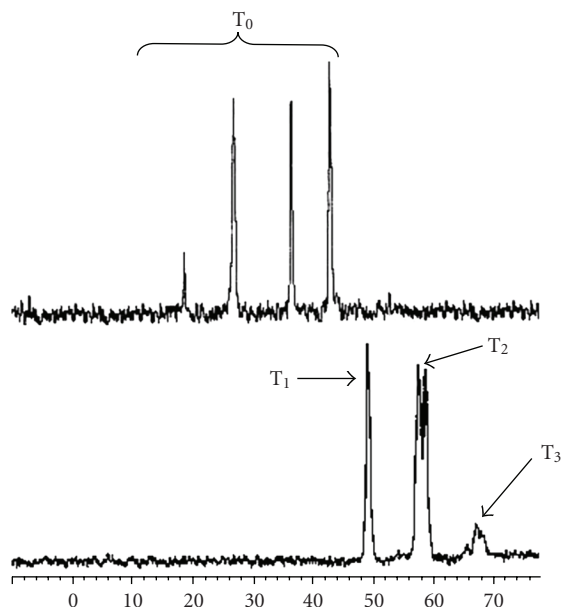
FIGURE 2: $^{29}$Si-NMR spectrum of sample after 1 hour and 24 hours of reaction.

TABLE 1

| Groups | % | Chemical shift (ppm) |
|---|---|---|
| RSiOMe3 | 33.7 | −42.8 |
| RSiOMe2Cl | 27 | −36.5 |
| RSiOMeCl2 | 30.3 | −27 |
| SiCl4 | 9 | −19.2 |

recorded after 1 hour of reaction are not attributable to any condensed silica species. As these peaks are located at chemical shifts located between those of the pure precursors, it is obvious that an exchange of the methoxy and chloride groups between both precursors has occurred, resulting in the formation of a mixture of organochlorosilane as shown in Table 1. Indeed, chloride is well known to be an electro-attractive group by inductive effect, which results in a decrease of the electronic density around the Si nuclei, explaining the displacement of the resonances of the hybrid precursor toward lower chemical shifts.

After 24 hours of reaction, the resonances observed are located in the region of condensed siloxane, previously identified between −50 and −100 ppm [20]. Furthermore, the progressive shift by ∼10 ppm suggests a progressive increase of the degree of condensation, as summarised in Table 2. At this stage, it is important to note the absence in both spectra of any band centred at ∼−40 ppm confirming the absence of any hydrolysed species. Indeed, in a previous study [20] on a similar material, we have highlighted the resonances of silanol groups (Si-OH) ∼−40 ppm. The present result confirms the success of our nonhydrolytic sol-gel synthesis in obtaining OH-free materials and eliminates any further implication of these groups in the degradation of fluorescence via quenching.
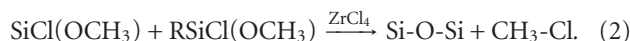
TABLE 2

| Groups | % | Chemical shift (ppm) |
|---|---|---|
| RSiOSi (T1) | 28.7 | −49.1 |
| RSi(OSi)2 (T2) | 55.3 | −58 |
| RSi(OSi)3 (T3) | 16 | −67 |

Furthermore, examination of these results suggests that the chemical reactions involved in this nonhydrolytic sol-gel synthesis can be divided into two steps.

The first implies the exchange of the chemical groups between both silanes:

$$SiCl_4 + RSi(OCH_3) \longrightarrow SiCl(OCH_3) + RSiCl(OCH_3). \quad (1)$$

The second step involves the $ZrCl_4$ catalyst in the formation of siloxane bonds. The most plausible reaction could involve the formation of an intermediate electronically deficient silicon nucleus that would be balanced by a hydrophylic species such as the oxygen contained in the methoxide group. This results in the formation of fully stable siloxane bonds and in the removal of volatile methyl chloride ($CH_3Cl$), as sketched in the following :

$$SiCl(OCH_3) + RSiCl(OCH_3) \xrightarrow{ZrCl_4} Si\text{-}O\text{-}Si + CH_3\text{-}Cl. \quad (2)$$

*3.2. Near-Infrared Spectroscopy.* Near infrared (NIR) spectra have been recorded on $Er^{3+}$ doped and $Er^{3+}/Yb^{3+}$ codoped samples. Figure 3 shows the NIR absorption of $Er^{3+}$ (0.5, 1 and 2% at) doped samples. Compared to the undoped sample [20], in which the absorption bands in this spectral range were ascribed to the first and second overtones of the CH groups, the main difference is the appearance of two bands located at 980 and 1540 nm.

Bands observed at 980 and 1540 nm are assigned to erbium transitions from the fundamental energy level to the excited levels $^4I_{11/2}$ and $^4I_{13/2}$, respectively. This is in agreement with the typical erbium absorption [21, 22]. 980 nm has been found to be the most favourable pumping wavelength as erbium-doped optical amplifiers display a quasi-quantum limited 3 dB noise level, while also displaying an improved performance in terms of gain efficiency [23]. In our material, the absorption at 980 nm is particularly weak at around 20% of the absorption measured at 1540 nm, even for the sample containing the highest erbium concentration. To increase this absorption, $Yb^{3+}$ ions can be employed as a codoping agent, as well known to exhibit a strong absorption at 980 nm [24]. When pumped at 980 nm, $Yb^{3+}$ ions are excited to the first energy level ($^2F_{5/2}$) and then relaxed to the ground level by nonradiative transition. However, in presence of $Er^{3+}$ ions, an energy transfer process from the excited $Yb^{3+}$ ions toward the $^2I_{13/2}$ level of the $Er^{3+}$ ions can take place to increase the population of the excited $Er^{3+}$ ions in this level, as sketched in (Figure 4). Indeed, because of the proximity of the ions energy levels, energy transfer is very efficient, as it is quasi-resonant. Since the population of the $^4I_{13/2}$ is increased by this mechanism, the luminescence lifetime of the $Er^{3+}$ ions on this energy level should also be increased and the resulting fluorescence intensity improved.
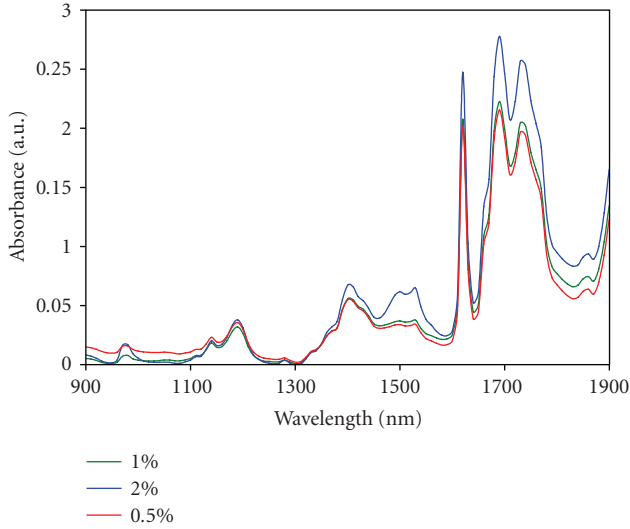
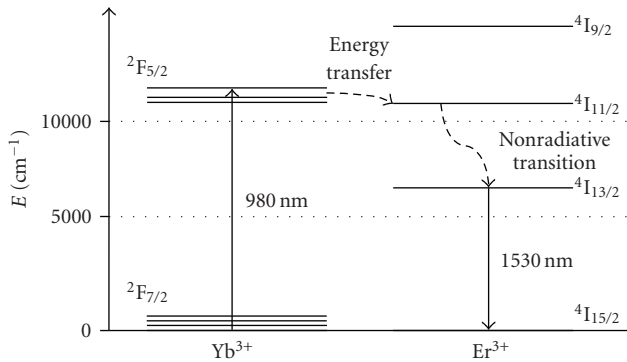FIGURE 3: Near-infrared spectra of $Er^{3+}$-doped samples (0.5, 1, and 2% at).



FIGURE 5: Near-infrared spectra of $Er^{3+}:Yb^{3+}$-codoped samples (0.5 : 6, 1 : 6, and 2 : 6% at).



FIGURE 4: Energy transfer between $Yb^{3+}$ and $Er^{3+}$ ions.

Figure 5 shows the NIR absorption spectra of $Er^{3+}/Yb^{3+}$ codoped monoliths (6% at $Yb^{3+}$). Compared to Figure 3, two observations are evident. Firstly, the absorption at 980 nm is increased by a factor of around 200. Secondly, the high erbium absorption around 1540 nm is strongly reduced by ∼ 80%, in all samples revealing interactions at the atomic level between both $Er^{3+}$ and $Yb^{3+}$ ions. The only explanation we found to this behaviour involves an up-conversion process from the $^4I_{13/2}$ to reach the $^4I_{11/2}$, by absorption of a second photon at 1540 nm. From this excited level, the $Er^{3+}$ ions can either undergo a nonradiative relaxation to the $^4I_{13/2}$ state followed by a radiative transition to the ground level or process a nonradiative transfer to neighbouring $Yb^{3+}$ ions ($^2F_{5/2}$ excited level). Comparison of Figures 3 and 5 clearly suggests the involvement of $Yb^{3+}$ ions in the up-conversion process of $Er^{3+}$ ions. However, to our knowledge, no study has previously reported the implication of $Yb^{3+}$ ions in the up-conversion process of the $Er^{3+}$ ions when excited at 1540 nm. This important physical process, highlighted for the first time in this paper, will be further investigated by the authors and further clarification will be proposed in a future study.
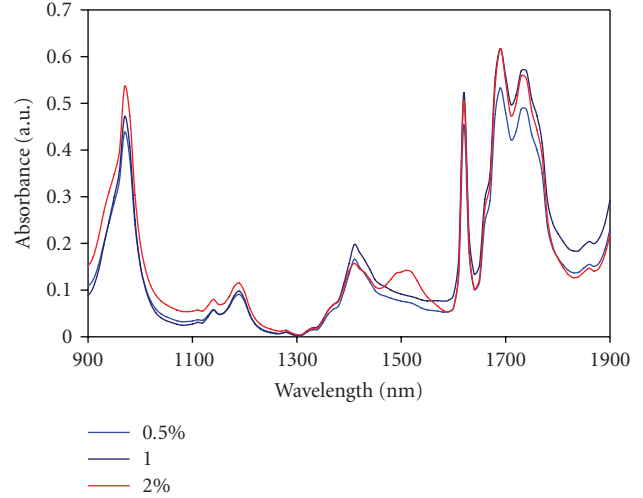
*3.3. Fluorescence.* Figure 6 shows the emission spectra in the near infrared region of $Er^{3+}/Yb^{3+}$ codoped bulk samples. $Er^{3+}$ and $Yb^{3+}$ are, respectively, pumped to the $^4I_{11/2}$ and $^2F_{5/2}$ excited levels employing a Ti: sapphire laser tuned to 980 nm. $Er^{3+}$ ions first decay nonradiatively to the $^4I_{13/2}$ level followed by a final decay to the ground state $^4I_{15/2}$ by emitting a photon at 1530 nm (Figure 5).

Both spectra show a main photoluminescence peak at 1530 nm and two shoulders around 1500 and 1550 nm with wide tails extending from roughly 1450 to 1650 nm. The peak shape is attributed to the stark splitting of the excited state $^4I_{13/2}$ and ground state $^4I_{15/2}$ of $Er^{3+}$ ions. Furthermore, the full width at half maximum is abnormally high at around 30 to 50 nm, which is on average of 30% higher than those measured in pure mineral materials [25, 26]. In a first instance, this can be explained by the amorphous structure of the matrix and the codoping with $Yb^{3+}$ ions. Oppositely to crystalline materials, which can precisely define the position of rare-earth ions within a host matrix, the amorphous nature of our glass-like material favours a random distribution, resulting in a broadening of the luminescence signal.

However, the measured photoluminescence intensity is very low for both samples, which we estimated at 1% of that generally obtained in the case of pure silica matrices. Insofar as the material does not contain any OH groups, quenching by these groups is then eliminated. From these results two hypotheses remain possible: firstly, autoquenching of the fluorescence due to agglomeration of the $Er^{3+}$ ions, secondly, the energy dissipation in the matrix caused by a multiphonon relaxation process. To understand the mechanism responsible for the relatively low level of measured fluorescence, we have studied the $Er^{3+}$ structure within the hybrid material by electron paramagnetic resonance and neutron scattering.

*3.4. Electron Paramagnetic Resonance.* EPR spectra of samples doped with $Er^{3+}$ at 0.5, 1, and 2% at are shown in
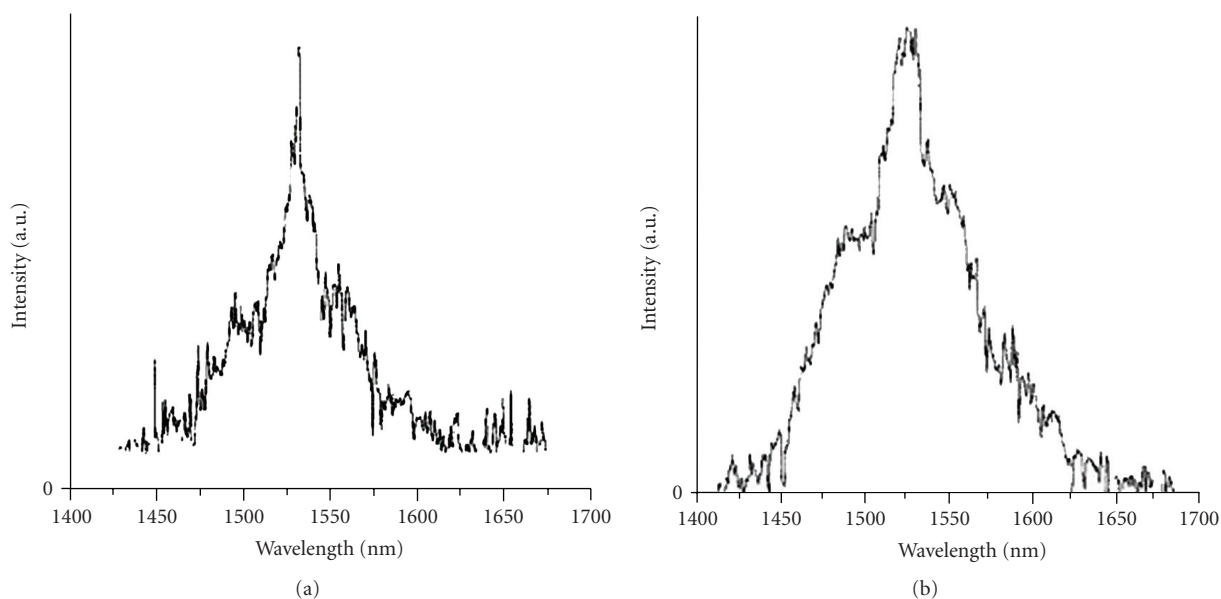
FIGURE 6: Room-temperature luminescence spectra in the near infrared region of $Er^{3+}/Yb^{3+}$-codoped samples ((a) 1/6 and (b) 2/6% at).
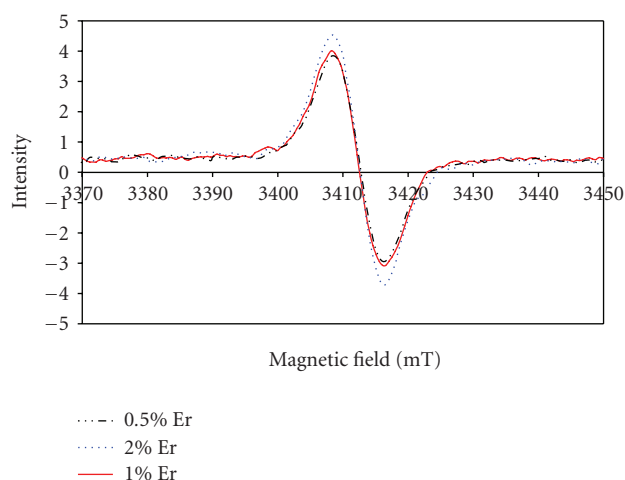


FIGURE 7: Electron paramagnetic resonance spectra of $Er^{3+}$ doped samples (0.5, 1, and 2% at).

Figure 7. A single signal was detected for magnetic fields varying from 0 to 4000 mT that exhibit a constant peak to peak width (~8mT) and a progressive increase of the intensity with the increase of the $Er^{3+}$ ion concentration.

To our knowledge, no literature reported any EPR results on $Er^{3+}$ ions incorporated in either organic polymers or hybrid materials to allow a direct comparison with similar amorphous structures. However, compared to $Er^{3+}$ ions incorporated in crystalline structures [27–29], the EPR signals obtained in our material require a magnetic field of approximately 4 times greater magnitude [30]. This suggests that the $Er^{3+}$ ions are strongly linked to the hybrid matrix.

As the paramagnetic character is preserved, the formation of covalent bonds between $Er^{3+}$ and the matrix is unlikely. However, physical interactions with the strong nucleophilic groups of the matrix can explain the observed behaviour. Indeed, the material contains oxygen atoms in the carboxylic functions that can potentially act as complexing agent by electron donor effect, then reducing the paramagnetic character of the active ions in the material.

Compared to crystalline structures that precisely define the position of the rare earth ion [30], the amorphous structure of the hybrid glass can potentially allow a random distribution of $Er^{3+}$ ions within the matrix. However, according to the EPR data, a single peak was observed indicating that the environment of the different $Er^{3+}$ ions in our material is very similar. However, the EPR technique does not give any information about the concentration effect on the evolution of the Er-Er interatomics distances. This is investigated using neutron scattering characterisation.

*3.5. Neutron Scattering.* Rare earth agglomerates have been reported with dimensions between a few angstroms to several nanometers [31]. Neutron scattering experiments have been conducted to yield information about any structural change associated with the possible formation of $Er^{3+}$ clusters.

Figure 8 shows the neutron scattering spectra for the undoped and $Er^{3+}$ doped samples with 0.5, 1 and 2% at All spectra exhibit a similar behaviour, with a single band the maximum of which was detected at a wavevector of $1.29.10^{-2}$, which progressively decreases with the increase of the dopant concentration.

The stability of the maximum band position confirms that the size structure of the material is invariant, and excludes the formation of any novel phase, whatever the dopant concentration is. This indicates that fluorescence autoquenching by energy transfer between neighbouring $Er^{3+}$ is not the prevalent relaxation process. Moreover, the decrease of the signal intensity is explained by the increase of the $Er^{3+}$ scattering.
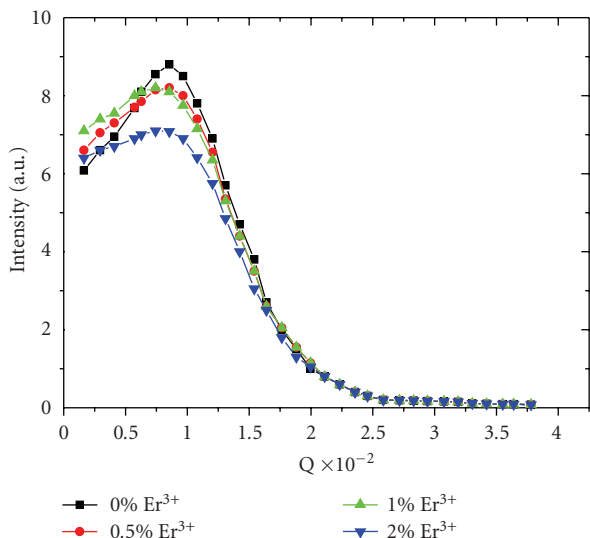
FIGURE 8: Neutron scattering spectra of un-doped and $Er^{3+}$ doped samples (0.5, 1, and 2% at).

Consequently, the weak fluorescence intensity measured is not due to nonradiative relaxation by either the erbium structure or OH groups. We propose that it is associated with the energy dissipation within the matrix by multiphonon nonradiative relaxation process. In our case, CH groups ($\nu$(C-H) $\sim$2800–3100 cm$^{-1}$) contained in the organic part of the hybrid, are the only species capable of competing with the radiative emission of $Er^{3+}$ ions around 1550 nm, by a two- or three-phonon relaxation process.

## 4. Conclusion

The approach developed in this paper aimed at establishing the material requirements for the development of future photocurable hybrid materials as rare earth host matrices for optical amplification applications.

An erbium doped organic-inorganic sol-gel material has been synthesised via a nonhydrolytic process leading to an OH-free material. The emission characterisation revealed low photoluminescence intensity estimated at about 0.1% of similar $Er^{3+}$ doped silica fibres used in the telecommunication industry.

Electron paramagnetic resonance and neutron scattering have been used to demonstrate a homogeneous distribution of $Er^{3+}$ ions within the hybrid structure, which excluded any autoquenching by energy transfer between $Er^{3+}$ neighbours atoms as an explanation for the low fluorescence. This result was then attributed to a multiphonon relaxation process involving the CH groups, in the organic part of the hybrid material. The development of future active materials for optical amplification requires taking into consideration 2 critical parameters. Firstly, the active rare earth ion needs to be nonlinked to any complexing agent that could drastically decrease its paramagnetic character, then strongly affecting the inversion of population toward its excited levels. Secondly, the structure of the host matrix

should be designed to minimise any energetic dissipation by multiphonon relaxation process. These conditions can potentially be fulfilled by the development of fluorinated organic hybrid materials, which vibrations are theoretically unable to compete with the desired radiative emission of the $Er^{3+}$ ions to further obtain a gain by optical amplification.

From an example of a classical hybrid organic-inorganic material, the approach developed in this paper aimed at establishing the material requirements for the development of future high performance materials applied to the development of optical integrated devices.

## References

[1] C. J. Brinker and G. W. Scherer, *Sol-Gel Science*, Academic Press, San Diego, Calif, USA, 1990.

[2] D. Gomes, S. P. Nunes, and K.-V. Peinemann, "Membranes for gas separation based on poly(1-trimethylsilyl-1-propyne)—silica nanocomposites," *Journal of Membrane Science*, vol. 246, no. 1, pp. 13–25, 2005.

[3] K. Maver, U. Lavrenčič Štangar, P. Judeinstein, and J. M. Zanotti, "Dynamic studies of Ormosil membranes," *Journal of Non-Crystalline Solids*, vol. 354, no. 2–9, pp. 680–687, 2008.

[4] P. C. Pandey, S. Upadhyay, I. Tiwari, G. Singh, and V. S. Tripathi, "A novel ferrocene encapsulated palladium-linked ormosil-based electrocatalytic dopamine biosensor," *Sensors and Actuators B*, vol. 75, no. 1-2, pp. 48–55, 2001.

[5] K. R. Kribich, R. Copperwhite, H. Barry, et al., "Novel chemical sensor/biosensor platform based on optical multimode interference (MMI) couplers," *Sensors and Actuators B*, vol. 107, no. 1, pp. 188–192, 2005.

[6] N. N. Voevodin, J. W. Kurdziel, and R. Mantz, "Corrosion protection for aerospace aluminum alloys by Modified Self-assembled NAnophase Particle (MSNAP) sol-gel," *Surface and Coatings Technology*, vol. 201, no. 3-4, pp. 1080–1084, 2006.

[7] R. Zandi-Zand, A. Ershad-Langroudi, and A. Rahimi, "Organic-inorganic hybrid coatings for corrosion protection of 1050 aluminum alloy," *Journal of Non-Crystalline Solids*, vol. 351, no. 14-15, pp. 1307–1311, 2005.

[8] P. Coudray, P. Etienne, and Y. Moreau, "Integrated optics based on organo-mineral materials," *Materials Science in Semiconductor Processing*, vol. 3, no. 5-6, pp. 331–337, 2000.

[9] W.-J. Ho, J.-S. Chen, M.-D. Ker, et al., "Fabrication of a miniature CMOS-based optical biosensor," *Biosensors and Bioelectronics*, vol. 22, no. 12, pp. 3008–3013, 2007.

[10] J. Porque, P. Coudray, R. Charters, K. Kribich, P. Etienne, and Y. Moreau, "WDM based on multimode interference-coupler built in an organic-inorganic material," *Optics Communications*, vol. 183, no. 1–4, pp. 45–49, 2000.

[11] M. Oubaha, M. Smaïhi, P. Etienne, P. Coudray, and Y. Moreau, "Spectroscopic characterization of intrinsic losses in an organic-inorganic hybrid waveguide synthesized by the sol-gel process," *Journal of Non-Crystalline Solids*, vol. 318, no. 3, pp. 305–313, 2003.

[12] M. Oubaha, P. Etienne, P. Boutinaud, J. M. Nedelec, P. Coudray, and Y. Moreau, "Improvement of the guiding performances of near infrared organic/inorganic channel waveguides," *Optical Materials*, vol. 28, no. 5, pp. 502–505, 2006.

[13] M. Oubaha, R. Copperwhite, B. Murphy, et al., "Development of photo-patternable organo-mineral hybrid films from the

sol-gel condensation of alkoxysilanes," *Thin Solid Films*, vol. 510, no. 1-2, pp. 334–338, 2006.

[14] A. J. Faber, D. R. Simmons, Y. Yan, and H. De Waal, "Photoluminescence quenching by OH in Er- and Pr-doped glasses for 1.5 and 1.3 $\mu$m optical amplifiers," in *Fiber Optic Materials and Components*, vol. 2290 of *Proceedings of SPIE*, p. 80, San Diego, Calif, USA, 1994.

[15] A. Beeby, I. M. Clarkson, R. S. Dickins, et al., "Non-radiative deactivation of the excited states of europium, terbium and ytterbium complexes by proximate energy-matched OH, NH and CH oscillators: an improved luminescence method for establishing solution hydration states," *Journal of the Chemical Society, Perkin Transactions 2*, no. 3, pp. 493–503, 1999.

[16] L. Bourget, R. J. P. Corriu, D. Leclercq, P. H. Mutin, and A. Vioux, "Non-hydrolytic sol-gel routes to silica," *Journal of Non-Crystalline Solids*, vol. 242, no. 2-3, pp. 81–91, 1998.

[17] Y. K. Sharma, S. S. L. Surana, R. K. Singh, and R. P. Dubedi, "Spectral studies of erbium doped soda lime silicate glasses in visible and near infrared regions," *Optical Materials*, vol. 29, no. 6, pp. 598–604, 2007.

[18] F. Babonneau and J. Maquet, "Nuclear magnetic resonance techniques for the structural characterization of siloxane-oxide hybrid materials," *Polyhedron*, vol. 19, no. 3, pp. 315–322, 2000.

[19] M. Oubaha, M. Smaïhi, P. Etienne, P. Coudray, and Y. Moreau, "Spectroscopic characterization of intrinsic losses in an organic-inorganic hybrid waveguide synthesized by the sol-gel process," *Journal of Non-Crystalline Solids*, vol. 318, no. 3, pp. 305–313, 2003.

[20] M. Oubaha, P. Etienne, S. Calas, R. Sempere, J. M. Nedelec, and Y. Moreau, "Spectroscopic characterization of sol-gel organo-siloxane materials synthesized from aliphatic and aromatic alcoxysilanes," *Journal of Non-Crystalline Solids*, vol. 351, pp. 2122–2128, 2005.

[21] Y. K. Sharma, S. S. L. Surana, R. K. Singh, and R. P. Dubedi, "Spectral studies of erbium doped soda lime silicate glasses in visible and near infrared regions," *Optical Materials*, vol. 29, no. 6, pp. 598–604, 2007.

[22] M. Oubaha, P. Etienne, S. Calas, P. Coudray, J. Nedelec, and Y. Moreau, "Sol-gel derived organic and inorganic hybrid materials for photonic applications: contribution to the correlation between the material structure and the transmission in the near infrared region," *Journal of Sol-Gel Science and Technology*, vol. 33, no. 2, pp. 241–248, 2005.

[23] R. I. Laming and D. N. Payne, "Noise characteristics of erbium-doped fiber amplifier pumped at 980 nm," *IEEE Photonics Technology Letters*, vol. 2, no. 6, pp. 418–421, 1990.

[24] A. Q. Le Quang, J. Zyss, I. Ledoux, et al., "An hybrid organic-inorganic approach to erbium-functionalized nanodots for emission in the telecom window," *Chemical Physics*, vol. 318, no. 1-2, pp. 33–43, 2005.

[25] M. Benatsou and M. Bouazaoui, "Fluorescence properties of sol-gel derived $Er^{3+}$:$SiO_2$-$GeO_2$ planar waveguides," *Optics Communications*, vol. 137, no. 1–3, pp. 143–150, 1997.

[26] F. A. Sigoli, R. R. Gonçalves, A. S. S. de Camargo, L. A. O. Nunes, Y. Messaddeq, and S. J. L. Ribeiro, "Preparation and characterization of erbium and ytterbium co-doped sol-gel $SiO_2$:$HfO_2$ films for planar waveguides," *Optical Materials*, vol. 30, no. 4, pp. 600–607, 2007.

[27] N. T. Bagraev, A. D. Bouravleuv, W. Gehlhoff, L. E. Klyachkin, A. M. Malyarenko, and V. V. Romanov, "Erbium-related centres embedded in silicon microcavities," *Physica B*, vol. 340–342, pp. 1074–1077, 2003.

[28] T. Bodziony and S. M. Kaczmarek, "EPR and optical measurements of weakly doped $LiNbO_3$: Er," *Physica B*, vol. 400, no. 1-2, pp. 99–105, 2007.

[29] P. G. Baranov, I. V. Ilyin, and E. N. Mokhov, "Electron paramagnetic resonance of the group-III deep acceptor impurities in SiC," *Solid State Communications*, vol. 100, no. 6, pp. 371–376, 1996.

[30] P. Boutinaud, E. Pinel, M. Oubaha, R. Mahiou, E. Cavalli, and M. Bettinelli, "Making red emitting phosphors with $Pr^{3+}$," *Optical Materials*, vol. 28, no. 1-2, pp. 9–13, 2006.

[31] F. Auzel, D. Meichenin, F. Pellé, and P. Goldner, "Cooperative luminescence as a defining process for RE-ions clustering in glasses and crystals," *Optical Materials*, vol. 4, no. 1, pp. 35–41, 1994.